Well performing Fe-SnO2 for CO2 reduction to HCOOH

Catalysis Communications 163 (2022) 106412

Contents lists available at ScienceDirect

Catalysis Communications

journal homepage: www.elsevier.com/locate/catcom

Well performing Fe-SnO_2 for CO_2 reduction to HCOOH

U. Savino [a,b,*], A. Sacco [a], K. Bejtka [a,b], M. Castellino [b], M.A. Farkhondehfal [a], A. Chiodoni [a], F. Pirri [a,b], E. Tresso [b]

[a] Center for Sustainable Future Technologies @ POLITO, Istituto Italiano di Tecnologia, Via Livorno 60, 10144 Turin, Italy
[b] Department of Applied Science and Technology, Politecnico di Torino, Corso Duca degli Abruzzi 24, 10129 Turin, Italy

ARTICLE INFO

Keywords:
Electrochemical CO_2 reduction
SnO_2 catalyst
Fe doping
HCOOH production
Anodic oxidation

ABSTRACT

The climate change imposes to mankind a severe management of CO_2 emissions in atmosphere. CO_2 valorization through electrocatalysis revealed to be a valuable solution to this global issue. SnO_2 is an electrocatalyst widely investigated for its capability to reduce CO_2 to formic acid. In particular, mesoporous SnO_2 offers a high adsorption capability, resulting in a high catalytic activity. In order to improve its performance, Fe-doping is here investigated for the first time. We observed that Fe-doped SnO_2 exhibits a remarkable 100% enhancement of the partial current density for HCOOH production at relatively low overpotentials, although keeping the selectivity unchanged.

1. Introduction

According to the Paris agreement, the control of climate change imposes a common effort among all the nations through the control and limitation of CO_2 emissions in atmosphere. In order to reach this goal, different strategies have been adopted. [1–3] Among them, catalytic CO_2 reduction reaction (CO_2RR) is the more valuable since it allows to convert CO_2 into a resource, namely a carbon-based fuel or a chemical.

Aiming to obtain a novel, well-performing, cheap and easily scalable catalyst, the attention has been focused on tin oxide (SnO_2) and its doped forms. Tin oxide is an attractive semiconductive material with high catalytic power and non-noble, eco-friendly and low-cost characteristics. [4] From the catalytic point of view, SnO_2 is particularly interesting because of its a high selectivity to formic acid (HCOOH). [5] From the perspective of a large-scale application of the catalyst, the selectivity would ease the CO_2RR product separation: the liquid HCOOH from the gaseous minor products (CO and H_2).

A great number of methods have been developed until now to prepare nanostructured SnO_2 catalysts [6–8] Among them, anodic-oxidation (AO) of tin foils unveiled to be a simple, high yield, low-cost, scalable, easily reproducible and effective strategy to prepare nanostructured porous materials. [9] As already demonstrated by Bejtka et al., [10] sponge-like SnO_2 realized via AO is capable to reduce CO_2 to formic acid with good selectivity.

The main chasing properties of a performing electrocatalyst are (i) the good selectivity through products, (ii) the low energy requirements, i.e. the lower the reaction over-potential the better, and (iii) the high electron transfer, which stands for high current densities at low bias. The applied potential for SnO_2-based catalysits is commonly more negative than −1 V vs Reversible Hydrogen Electrode (RHE). Only few works are reported in literature with a lower overpotential (around −0.8 V vs RHE). As an example, Kumar et al. [7] realized SnO_2 nanoparticles capable to reduce CO_2 to HCOOH at −0.8 V vs RHE, although with a partial current of just −1.4 mA/cm^2. A similar result was obtained by the same group with porous nanowalls, [7] and by Ge et al. [11] with mesoporous structures. In order to reach higher partial currents, the potential has to be more negative. Partial current denisties over −10 mA/cm^2 were reached with Sn dendrite [12] and chainlike mesoporous SnO_2, [10] but with applied potentials lower than −1.1 V vs RHE.

To overcome these limitations, doping has been investigated [13,14] as a possible way to induce nanostructure modification, together with the density of states engineering to push the catalytic properties of SnO_2 toward CO_2 reduction at lower overpotentials.

As proved by literature, in systems containing metals, like Au and Cu, the broken spatial symmetry near grain boundaries changes the binding energy of the reaction intermediates, facilitating the CO_2 reduction to CO [15] and its reduction to C_{2+} products, [16] thus arousing the attention in the study of modified-SnO_2. The effect of doping results in an upward shift in the Pourbaix diagram boundary separating the [3H/1CO_2] and [4H/1CO_2] states. This means that dopants should lower the

* Corresponding author at: Center for Sustainable Future Technologies @ POLITO, Istituto Italiano di Tecnologia, Via Livorno 60, 10144 Turin, Italy.
E-mail address: umbe.sav@gmail.com (U. Savino).

https://doi.org/10.1016/j.catcom.2022.106412
Received 17 September 2021; Received in revised form 16 January 2022; Accepted 21 January 2022
Available online 24 January 2022

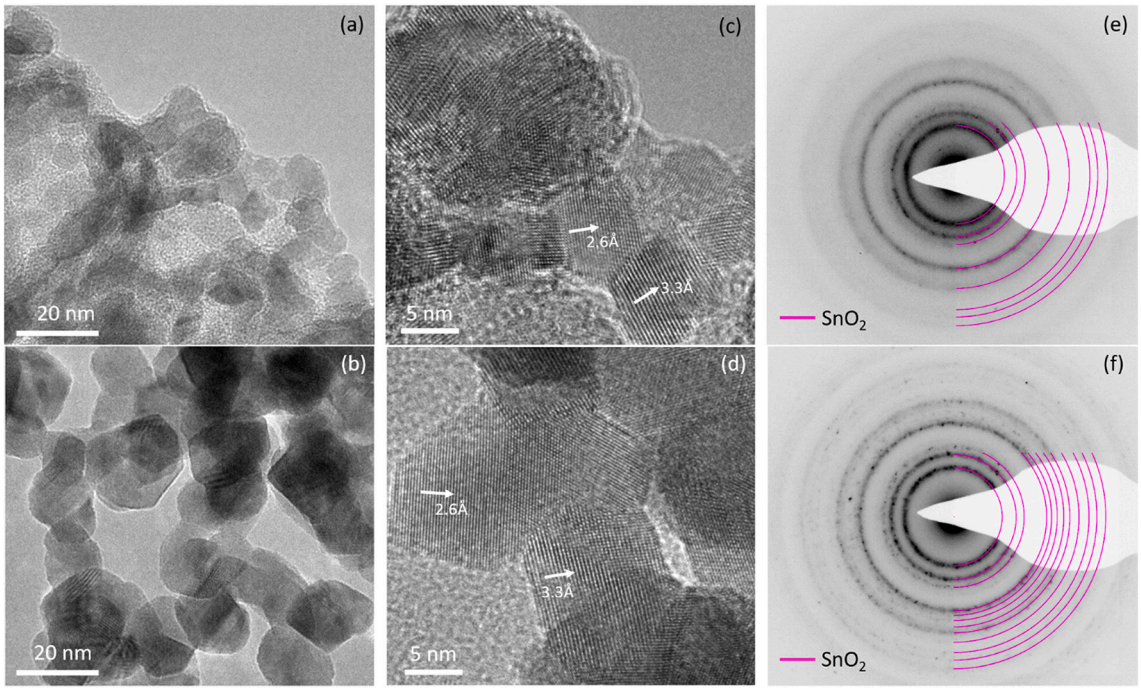

Fig. 1. TEM characterization: BF-TEM (a, b) HR-TEM (c, d) and SAED (e, f) for SnO_2 (a, c, e) and Fe-SnO_2 (b, d, f) respectively. In HR-TEM images interplanar spacings calculated from FFT (not shown) are provided (~3.3 Å (110), ~2.6 Å (101) family of planes of the SnO_2 structure). In SAED images a simulated pattern for SnO_2 crystal structure is also shown.

over-potential for CO_2 reduction with respect to un-doped tin oxide. For this reason, doping has been suggested by Saravanan et al. [14] as good strategy for future experimental investigations on energetically efficient CO_2 reduction.

We selected Fe-doping because the inclusion of Fe^{3+} ion is expected to induce a p-type behaviour in SnO_2, thus increasing the resistivity of the material [20–22], and to introduce oxygen vacancies [22,23] which are beneficial for CO_2RR. Albeit Fe-doped SnO_2 has been already investigated for different applications, [17–23] to the best of our knowledge it has never been studied as electrocatalyst for CO_2RR.

SnO_2 was synthesized via AO, following the procedure presented by Bejtka et al. [10]. The doping has been attained following the procedure developed by Jain et al. [24] on Ni-doped SnO_2 (synthesis reported in the SI). The same dopant molar concentration and synthesis parameters were kept in order to establish a starting procedure. A complete structural characterization has been carried on. Fe-doped SnO_2 has been then tested as electrocatalyst for CO_2RR. As a result, the material exhibits a good selectivity toward formic acid (HCOOH) with a secondary production of CO and H_2. The selectivity toward HCOOH and CO is taken as a great advantage since they are easily separable; moreover, CO and H_2 can be employed to obtain syngas. [25]

2. Results and discussion

2.1. Material characterization

The un-doped SnO_2 samples annealed at 600 °C display a porous and irregular structure (Fig. S1 a–b), composed by nanochannels, with about 50 nm mean diameter and wall thickness of about 15 nm, which is typical for SnO_2 prepared by anodic oxidation. [10] The TEM characterization shown in Fig. 1 a and c gives more detailed information on morphological and structural properties. The bright field (BF) and HR-TEM show that the pore walls are made of small-interconnected crystals, with a size in the range of 5–20 nm. The ring pattern in Selected Area Electron Diffraction (SAED), analyzed with the Circular Hough analysis tool [26] of Digital Micrograph™ software, confirms the polycrystalline nature of the sample, and the crystalline phase present of SnO_2 (tin oxide, JCPDS 00–041-1445).

The mesoporous structure, created during the synthetic process, allow the easy access of the electrolyte to the catalytic sites and efficient mass diffusion. [11] Moreover, the nanostructuration with tailored surface configuration proved to be an effective strategy to enhance the catalytic activity. [15,16]

Vertically aligned nanochannels were observed in SnO_2 realized by anodic oxidation by the group of Palacios-Padròs [27] and in our previous work, [10] with fully open pores, whose diameter is compatible with the one we measured. This implies that the increase of the annealing temperature to 600 °C (necessary for the doping step) does not affect the sample morphology.

The introduction of Fe doping into SnO_2 sample leads to the formation of bigger crystals, with good crystallinity (Fig. 1e), clearly discernible in the FESEM (Fig. S1 c) and BF-TEM (Fig. 1d) images. The increased crystal-size, which, on the basis of HR-TEM images, is of about 12–35 nm, causes the closure of the channels, which are no more discernible in the top-view FESEM image (Fig. S1 c). The structural characterization by SAED shows the ring pattern with reflections from numerous SnO_2 planes (tin oxide, JCPDS 00–041-1445), with no significant distortion to the unit cell. Although there is no detectable evidence of the dopant in the diffraction pattern, the EDX analysis confirms the presence of Fe in the doped-SnO_2 powder samples, as shown in Fig. S2. The lack of any evidence of the presence of metal clusters neither in HR-TEM nor in SAED suggests the dopants are well spread and completely inserted in the SnO_2 lattice.

A further investigation of the crystalline structure of the SnO_2 samples was carried out with XRD in Bragg-Brentano configuration. The obtained patterns correspond to SnO_2 (JCPDS 00–041-1445) with no significant variations of peak positions among the doped and un-doped samples (Fig.S3). The peak shape and FWHM in the un-doped sample give evidence of small coherent diffraction domains in this sample. Narrower peaks observed in Fe-SnO_2, which according to the Scherrer equation, give the evidence of increased size of coherent diffraction domains with respect to the un-doped sample, and this is consistent with

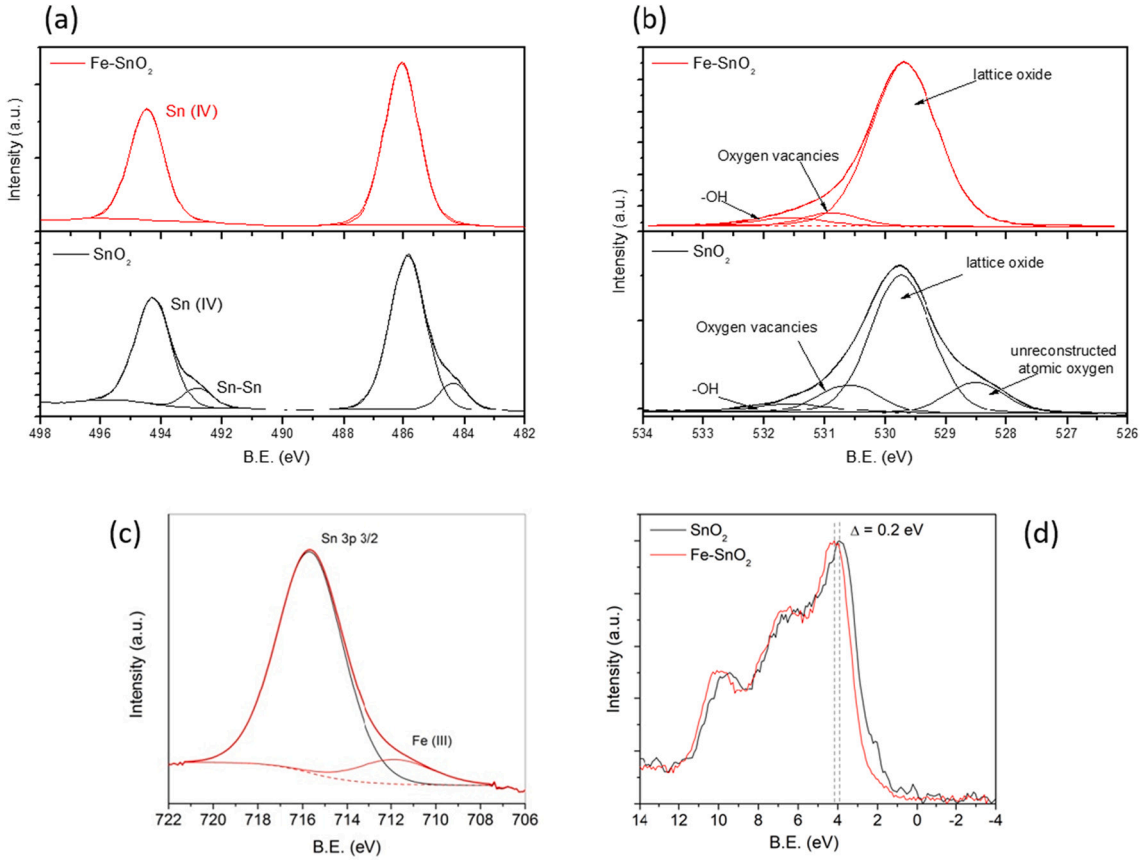

Fig. 2. XPS spectra of Sn 3d and O 1 s orbitals of SnO2 (a) and Fe-SnO_2 (b) respectively. Fe 2p of Fe-SnO_2 sample (c) and valence band spectra (d) are also shown. For sake of clarity, the spectra referred to SnO_2 are black, while the ones related to Fe-SnO_2 are red. (For interpretation of the references to colour in this figure legend, the reader is referred to the web version of this article.)

the TEM observation. The result is also in good agreement with the outcomes of Kaur et al. who found that Fe incorporation in SnO_2 lattice resulted in increasing grains size. [28]

Concerning the surface chemical composition, SnO_2 samples were characterized with XPS, using C 1 s peak (284.5 eV) to calibrate the spectra.

The survey spectra are reported in Fig. S4; Sn and O were observed in both samples, with small traces of adventitious carbon. Fe has been observed in the Fe-SnO_2 samples, which is consistent with the EDX results.

The Sn 3d doublet of SnO_2 sample is located at 485.9 eV (Sn $3d_{5/2}$) and 494.3 eV (Sn $3d_{3/2}$) as shown in Fig. 2 a. Since the peaks due to Sn (II) and Sn (IV) are close to each other, it is not trivial to distinguish the oxidation state of the compound. For this reason, the valence band (VB) shape has been used for the identification: as shown in Fig 2 d, the VB region displays the typical SnO_2 three-peaked structure. [29] Thus the most abundant oxidation state results to be Sn (IV), as also suggested by the 8.4 eV peaks distance related to the spin-orbit split. [10]

The small shoulders at lower binding energy (484.4 eV and 492.8 eV) can be ascribed to Sn—Sn, as reported by R. Shiratsuchi et al. [30]

The O 1 s spectrum (Fig. 2 b) confirms the presence of lattice oxide, displaying a strong component located at 529.7 eV, a small contribution due to O surface vacancies at 530.6 eV and a smaller component due to –OH species, as defined by the component at 531.5 eV. [31] A further peak located at 528.5 eV can be ascribed to unreconstructed atomic Oxygen, as reported by T.E. Jones et al. [32]

As regard Fe-SnO_2, the shift due to Sn—Sn bond in Sn3d doublet (see Fig. 2 a) and the peak due to O1s lowest chemical shift at 528.5 eV (Fig. 2 b) are disappeared. For both samples the presence of the Oxygen vacancy related peak is of fundamental importance since for application in CO_2 valorisation, oxygen vacancies are believed to participate in the catalysis by enhancing CO_2 adsorption and, as a consequence, its reduction.

As regard the dopant (Fig. 2 c), the peak maximum of Fe $2p_{3/2}$ stands at 711.7 eV. The position is connected to the oxidation state of Fe (III), [33] thus suggesting that iron was successfully inserted in the oxide structure. The close peak, located at 715.5 eV is referred to Sn $3p_{3/2}$, which is partially overlapping the Fe 2p doublet, as also observed by Xing et al. [34]

By looking at the VB region (Fig. 2 d), a 0.2 eV shift at higher binding energies has been observed for Fe-SnO_2. A similar outcome has been already published in literature by Egdell et al. [35] in their study concerning Sb-doped SnO_2 materials. In their findings the experimental results were explained by the presence of segregated doping atoms at the surface, a phenomenon which induces a shrinkage in the energy gap and a subsequent shift toward higher binding energies of the VB onset, thus proving the doping achievement.

2.2. *Electrochemical and CO_2 reduction tests*

Prior to CO_2RR test, CV has been carried out to first check the performances of the doped and un-doped samples. The CV plot in Fig. S5 shows that with equal potential, Fe-SnO_2 exhibits a higher current than SnO_2, which means that the Fe-doped electrodes have higher activity (higher geometric current).

The doped and un-doped SnO_2 samples have been, then, tested for CO_2RR in the same potential range (from −0.69 to −0.89 V vs RHE), and the production of formic acid has been analyzed.

As a result, the un-doped SnO_2 exhibits a maximum of HCOOH production, 40.0% of Faradaic efficiency (FE, eq. S1), at −0.89 V vs RHE

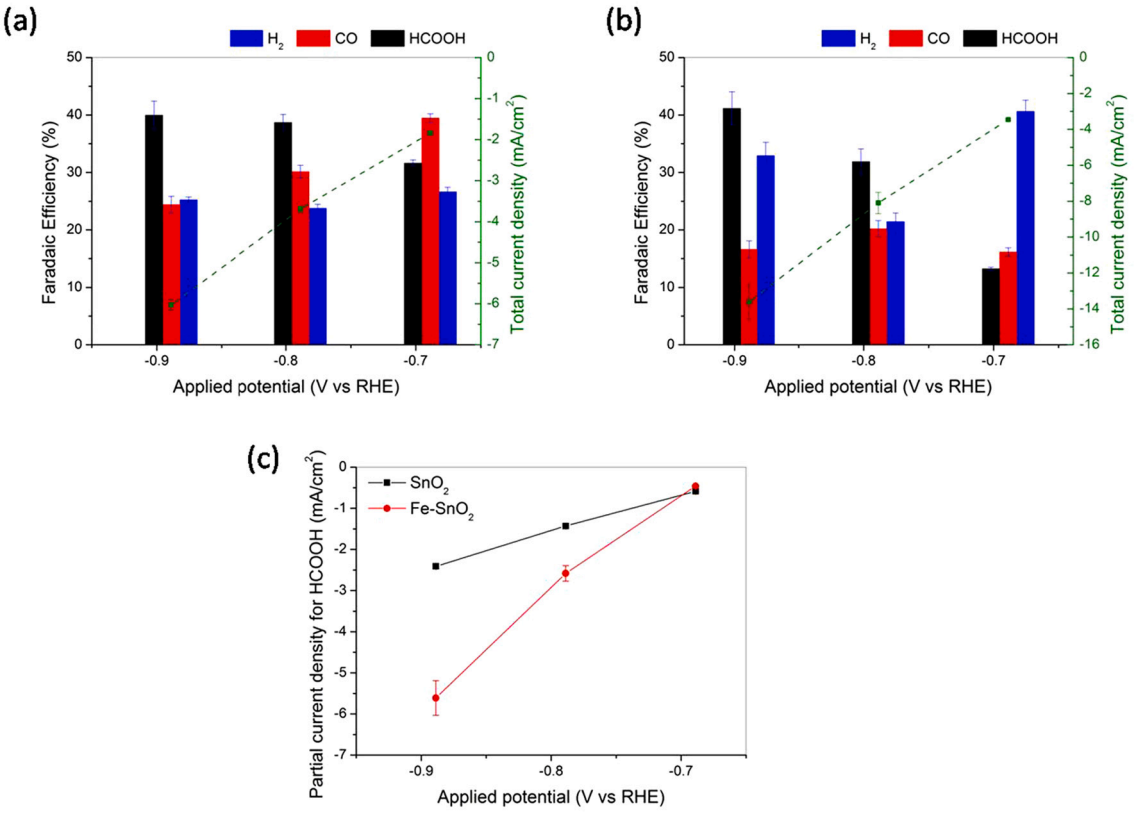

Fig. 3. Bar chart representing the Faradaic efficiencies for SnO_2 (a) and Fe-SnO_2 (b) for each tested potential. In green, the current density curve shows the behaviour at different applied potentials. (c) Partial current densities related to HCOOH production. (For interpretation of the references to colour in this figure legend, the reader is referred to the web version of this article.)

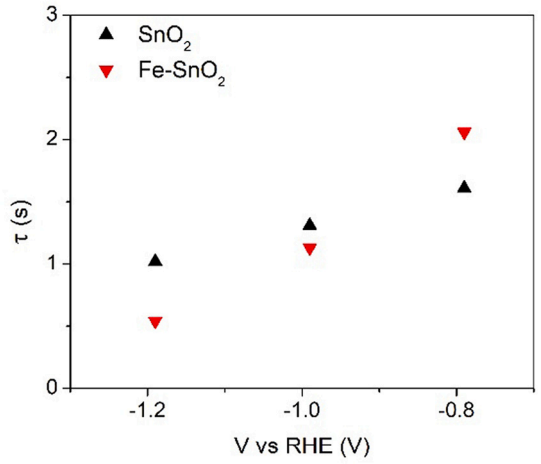

Fig. 4. Charge transfer time calculated for SnO_2 and Fe-SnO_2.

with a secondary production of H_2 and CO (Fig. 3 a). A stable total current density of -6.0 mA/cm^2 is obtained during 1 h of CO_2 reduction as shown in Fig. S6. The resulting FE is compatible to the one reported by Ge et al. [11] on mesoporous SnO_2, albeit with lower current densities. Moreover, the FE for HCOOH production is lower with respect to our previous work on SnO_2 electrocatalyst calcined at 450 °C; [10] however, it is woth notice that the over-potential corresponding to maximum HCOOH production has been lowered in the present work.

Similarly, Fe-SnO_2 exhibits the maximum of HCOOH production at the same potential (-0.89 V vs RHE) with a FE of 41% (Fig. 3 b). At this potential, CO_2 is reduced mainly to HCOOH, with H_2 and CO as secondary products. It is worth noting that the total current density of Fe-SnO_2 is more than two times higher than SnO_2, with a value at the equilibrium of -14 mA/cm^2. Thus, keeping the same selectivity of bare SnO_2, it is possible to double the efficiency of CO_2 reduction, as evident from the HCOOH partial current densities calculated trough eq. S2 (Fig. 3 c), to easily separable products. As expected, while the applied potential negatively increases, the equilibrium of the reaction moves from CO_2 reduction to H_2 evolution: for this reason, potentials more negative than -0.89 V vs RHE have not been investigated (further discussion on the reaction mechanism in the Supporting Information). The low overpotential makes the sample particularly interesting, especially for its relatively high current. The obtained high activity for HCOOH production (5.44 mA/cm^2) results to be among the highest ever reported for tin-oxide based electrocatalysts at potentials higher than -1 V vs RHE, as reported in Table S1.

The performance of Fe-SnO_2 has been investigated via EIS. By analyzing the impedance of both the samples (Fig. S7), a different behaviour of the charge transfer kinetics has been observed at the catalyst/electrolyte interface. In fact, by looking at the transfer time (Fig. 4), it is possible to observe a faster kinetic for Fe-SnO_2 with respect to bare SnO_2 while the potential is increasing. This imply that, in the former catalyst, a larger number of charges is available at the surface for the reduction reactions.

This result confirm that Fe-doping is an effective strategy in improving the performance of SnO_2 catalyst for CO_2RR.

3. Conclusion

A cheap and easily scalable technique to fabricate Fe-doped SnO_2 has been presented. The material has been tested for the first time for CO_2RR and demonstrated to be a valuable electrocatalyst for HCOOH

production. The highly porous structure, observed with FESEM, offers a high concentration of catalytic centres per unit area. Moreover, the presence of Fe-doping, confirmed by XPS analysis, demonstrated to be capable to keep the same selectivity of SnO_2, but increasing the production rate. In fact, a 100% enhancement of current density was observed at a relatively low potential of −0.89 V. The analysis of the impedance through EIS allowed to explain the result showing a faster charge transfer of Fe-SnO_2 sample with respect to SnO_2. In order to complete the investigation on the catalyst, stability tests will be carried out and the results will be presented in a future broader publication.

Although a further optimization of the catalyst is still possible, nevertheless, Fe-doped SnO_2 demonstrates to be a promising material for future technologies for CO_2RR.

Data availability

The data are available by contacting the corresponding author.

Author contribution and ORCID

Umberto Savino (ORCID: 0000-0003-1884-2444).

Conceptualization and synthesis of the materials. Electrochemical measurements, gas-products measurement, data analysis and interpretation.

Adriano Sacco (ORCID: 0000-0002-9229-2113).

EIS data analysis and interpretation.

Katarzyna Bejtka (ORCID: 0000-0003-1731-5861).

Undoped-catalyst conceptualization. Electron microscopy measurements (SEM and TEM), EDX measurements, data analysis and interpretation.

Micaela Castellino (ORCID: 0000-0002-1393-4043).

XPS measurements, data analysis and interpretation.

M. Amin Farkhondehfal (ORCID: 0000-0002-5433-5653).

HPLC measurements, data analysis and interpretation.

Angelica Chiodoni (ORCID: 0000-0002-4386-842×).

XRD measurements, data analysis and interpretation.

Fabrizio Pirri.

P.I. of IIT–CSFT@Polito scientific research line.

Elena Tresso (ORCID: 0000-0001-9223-379×).

First author's supervisor.

Funding sources

This research did not receive any specific grant from funding agencies in the public, commercial, or not-for-profit sectors.

Declaration of Competing Interest

The authors declare that they have no known competing financial interests or personal relationships that could have appeared to influence the work reported in this paper.

Acknowledgments

Authors acknowledge support from Enrico Savino for the realization of the tools required for electrochemical testing.

Appendix A. Supplementary data

Supplementary data to this article can be found online at https://doi.org/10.1016/j.catcom.2022.106412.

References

[1] M. van der Spek, T. Fout, M. Garcia, V.N. Kuncheekanna, M. Matuszewski, S. McCoy, J. Morgan, S.M. Nazir, A. Ramirez, S. Roussanaly, E.S. Rubin, Uncertainty analysis in the techno-economic assessment of CO_2 capture and storage technologies. Critical review and guidelines for use, Int. J. Greenh. Gas Control. 100 (2020), 103113, https://doi.org/10.1016/J.IJGGC.2020.103113.

[2] I.S. Omodolor, H.O. Otor, J.A. Andonegui, B.J. Allen, A.C. Alba-Rubio, Dual-function materials for CO_2 capture and conversion: a review, Ind. Eng. Chem. Res. 59 (2020) 17612–17631, https://doi.org/10.1021/ACS.IECR.0C02218.

[3] S. Zhang, Q. Fan, R. Xia, T.J. Meyer, CO_2 reduction: from homogeneous to heterogeneous electrocatalysis, Acc. Chem. Res. 53 (2020) 255–264, https://doi.org/10.1021/ACS.ACCOUNTS.9B00496.

[4] S. Zhao, S. Li, T. Guo, S. Zhang, J. Wang, Y. Wu, Y. Chen, Advances in Sn-based catalysts for electrochemical CO_2 reduction, Nano-Micro Lett. 11 (2019), https://doi.org/10.1007/s40820-019-0293-x.

[5] Q. Li, X. Rao, J. Sheng, J. Xu, J. Yi, Y. Liu, J. Zhang, Energy storage through CO_2 electroreduction: a brief review of advanced Sn-based electrocatalysts and electrodes, J. CO2 Util. 27 (2018) 48–59, https://doi.org/10.1016/j.jcou.2018.07.004.

[6] F. Li, L. Chen, G.P. Knowles, D.R. MacFarlane, J. Zhang, Hierarchical mesoporous SnO_2 nanosheets on carbon cloth: a robust and flexible electrocatalyst for CO_2 reduction with high efficiency and selectivity, Angew. Chem. Int. Ed. 56 (2017) 505–509, https://doi.org/10.1002/anie.201608279.

[7] B. Kumar, V. Atla, J.P. Brian, S. Kumari, T.Q. Nguyen, M. Sunkara, J.M. Spurgeon, Reduced SnO_2 porous nanowires with a high density of grain boundaries as catalysts for efficient electrochemical CO_2-into-HCOOH conversion, Angew. Chem. Int. Ed. 56 (2017) 3645–3649, https://doi.org/10.1002/anie.201612194.

[8] H. Hu, L. Gui, W. Zhou, J. Sun, J. Xu, Q. Wang, B. He, L. Zhao, Partially reduced Sn/SnO_2 porous hollow fiber: a highly selective, efficient and robust electrocatalyst towards carbon dioxide reduction, Electrochim. Acta 285 (2018) 70–77, https://doi.org/10.1016/j.electacta.2018.08.002.

[9] M. Wang, Y. Liu, D. Xue, D. Zhang, H. Yang, Preparation of nanoporous tin oxide by electrochemical anodization in alkaline electrolytes, Electrochim. Acta 56 (2011) 8797–8801, https://doi.org/10.1016/j.electacta.2011.07.085.

[10] K. Bejtka, J. Zeng, A. Sacco, M. Castellino, S. Hernández, M.A. Farkhondehfal, U. Savino, S. Ansaloni, C.F. Pirri, A. Chiodoni, Chainlike mesoporous SnO_2 as a well-performing catalyst for electrochemical CO_2 reduction, ACS Appl. Energy Mater. 2 (2019) 3081–3091, https://doi.org/10.1021/acsaem.8b02048.

[11] H. Ge, Z. Gu, P. Han, H. Shen, A.M. Al-Enizi, L. Zhang, G. Zheng, Mesoporous tin oxide for electrocatalytic CO_2 reduction, J. Colloid Interface Sci. 531 (2018) 564–569, https://doi.org/10.1016/j.jcis.2018.07.066.

[12] D.H. Won, C.H. Choi, J. Chung, M.W. Chung, E.H. Kim, S.I. Woo, Rational Design of a hierarchical tin dendrite electrode for efficient electrochemical reduction of CO_2, ChemSusChem. 8 (2015) 3092–3098, https://doi.org/10.1002/cssc.201500694.

[13] K. Bejtka, N.B.D. Monti, A. Sacco, M. Castellino, S. Porro, M.A. Farkhondehfal, J. Zeng, C.F. Pirri, A. Chiodoni, Zn- and Ti-doped SnO_2 for enhanced electroreduction of carbon dioxide, Materials (Basel). 14 (2021), https://doi.org/10.3390/ma14092354.

[14] K. Saravanan, Y. Basdogan, J. Dean, J.A. Keith, Computational investigation of CO_2 electroreduction on tin oxide and predictions of Ti, V, Nb and Zr dopants for improved catalysis, J. Mater. Chem. A 5 (2017) 11756–11763, https://doi.org/10.1039/c7ta00405b.

[15] K.S. Kim, W.J. Kim, H.K. Lim, E.K. Lee, H. Kim, Tuned chemical bonding ability of au at grain boundaries for enhanced electrochemical CO_2 reduction, ACS Catal. 6 (2016) 4443–4448, https://doi.org/10.1021/acscatal.6b00412.

[16] X. Feng, K. Jiang, S. Fan, M.W. Kanan, A direct grain-boundary-activity correlation for CO electroreduction on Cu nanoparticles, ACS Cent. Sci. 2 (2016) 169–174, https://doi.org/10.1021/acscentsci.6b00022.

[17] N. Lavanya, C. Sekar, S. Ficarra, E. Tellone, A. Bonavita, S.G. Leonardi, G. Neri, A novel disposable electrochemical sensor for determination of carbamazepine based on Fe doped SnO_2 nanoparticles modified screen-printed carbon electrode, Mater. Sci. Eng. C 62 (2016) 53–60, https://doi.org/10.1016/j.msec.2016.01.027.

[18] M.S. Pereira, F.A.S. Lima, T.S. Ribeiro, M.R. da Silva, R.Q. Almeida, E.B. Barros, I. F. Vasconcelos, Application of Fe-doped SnO_2 nanoparticles in organic solar cells with enhanced stability, Opt. Mater. (Amst). 64 (2017) 548–556, https://doi.org/10.1016/j.optmat.2017.01.023.

[19] F. Mueller, D. Bresser, V.S.K. Chakravadhanula, S. Passerini, Fe-doped SnO_2 nanoparticles as new high capacity anode material for secondary lithium-ion batteries, J. Power Sources 299 (2015) 398–402, https://doi.org/10.1016/j.jpowsour.2015.08.018.

[20] Z. Wang, L. Liu, Synthesis and ethanol sensing properties of Fe-doped SnO_2 nanofibers, Mater. Lett. 63 (2009) 917–919, https://doi.org/10.1016/j.matlet.2009.01.051.

[21] S. Bose, S. Chakraborty, B.K. Ghosh, D. Das, A. Sen, H.S. Maiti, Methane sensitivity of Fe-doped SnO_2 thick films, Sensors Actuators B Chem. 105 (2005) 346–350, https://doi.org/10.1016/j.snb.2004.06.023.

[22] D. Toloman, A. Popa, M. Stan, C. Socaci, A.R. Biris, G. Katona, F. Tudorache, I. Petrila, F. Iacomi, Reduced graphene oxide decorated with Fe doped SnO_2 nanoparticles for humidity sensor, Appl. Surf. Sci. 402 (2017) 410–417, https://doi.org/10.1016/j.apsusc.2017.01.064.

[23] W. Ben Haj Othmen, N. Sdiri, H. Elhouichet, M. Férid, Study of charge transport in Fe-doped SnO_2 nanoparticles prepared by hydrothermal method, Mater. Sci. Semicond. Process. 52 (2016) 46–54, https://doi.org/10.1016/j.mssp.2016.05.010.

[24] K. Jain, R.P. Pant, S.T. Lakshmikumar, Effect of Ni doping on thick film SnO_2 gas sensor, Sensors Actuators B Chem. 113 (2006) 823–829, https://doi.org/10.1016/j.snb.2005.03.104.

[25] S. Hernández, M.A. Farkhondehfal, F. Sastre, M. Makkee, G. Saracco, N. Russo, Syngas production from electrochemical reduction of CO_2: current status and prospective implementation, Green Chem. 19 (2017) 2326–2346, https://doi.org/10.1039/c7gc00398f.

[26] D.R.G. Mitchell, Circular Hough transform diffraction analysis: a software tool for automated measurement of selected area electron diffraction patterns within digital micrographTM, Ultramicroscopy. 108 (2008) 367–374, https://doi.org/10.1016/j.ultramic.2007.06.003.

[27] A. Palacios-Padrós, M. Altomare, A. Tighineanu, R. Kirchgeorg, N.K. Shrestha, I. Díez-Pérez, F. Caballero-Briones, F. Sanz, P. Schmuki, Growth of ordered anodic SnO_2 nanochannel layers and their use for H_2 gas sensing, J. Mater. Chem. A 2 (2014) 915–920, https://doi.org/10.1039/c3ta13704j.

[28] J. Kaur, J. Shah, R.K. Kotnala, K.C. Verma, Raman spectra, photoluminescence and ferromagnetism of pure, co and Fe doped SnO_2 nanoparticles, Ceram. Int. 38 (2012) 5563–5570, https://doi.org/10.1016/j.ceramint.2012.03.075.

[29] A. Cabot, J. Arbiol, R. Ferré, J.R. Morante, F. Chen, M. Liu, Surface states in template synthesized tin oxide nanoparticles, J. Appl. Phys. 95 (2004) 2178–2180, https://doi.org/10.1063/1.1639946.

[30] R. Shiratsuchi, K. Hongo, G. Nogami, S. Ishimaru, Reduction of CO_2 on fluorine-doped SnO_2 thin-film electrodes, J. Electrochem. Soc. 139 (1992) 2544–2549, https://doi.org/10.1149/1.2221260.

[31] J.Y.Y. Loh, N.P. Kherani, X-ray photospectroscopy and electronic studies of reactor parameters on photocatalytic hydrogenation of carbon dioxide by defect-laden indium oxide hydroxide nanorods, Molecules. 24 (2019), https://doi.org/10.3390/molecules24213818.

[32] T.E. Jones, T.C.R. Rocha, A. Knop-Gericke, C. Stampfl, R. Schlögl, S. Piccinin, Insights into the electronic structure of the oxygen species active in alkene epoxidation on silver, ACS Catal. 5 (2015) 5846–5850, https://doi.org/10.1021/acscatal.5b01543.

[33] M.C. Biesinger, B.P. Payne, A.P. Grosvenor, L.W.M. Lau, A.R. Gerson, R.S.C. Smart, Resolving surface chemical states in XPS analysis of first row transition metals, oxides and hydroxides: Cr, Mn, Fe, co and Ni, Appl. Surf. Sci. 257 (2011) 2717–2730, https://doi.org/10.1016/j.apsusc.2010.10.051.

[34] H. Xing, Z. Liu, L. Lin, L. Wang, D. Tan, Y. Gan, X. Ji, G. Xu, Excellent microwave absorption properties of Fe ion-doped SnO_2/multi-walled carbon nanotube composites, RSC Adv. 6 (2016) 41656–41664, https://doi.org/10.1039/c6ra04589h.

[35] R.G. Egdell, J. Rebane, T.J. Walker, D.S.L. Law, Competition between initial- and final-state effects in valence- and core-level x-ray photoemission of Sb-doped SnO_2, Phys. Rev. B 59 (1999) 1792–1799, https://doi.org/10.1103/PhysRevB.59.1792.